ACS APPLIED MATERIALS & INTERFACES

Research Article

Cite This: ACS Appl. Mater. Interfaces 2018, 10, 27308−27315

www.acsami.org

Photoactivated Polymeric Bilayer Actuators Fabricated via 3D Printing

Daniel E. Hagaman,[†] Steven Leist,[‡] Jack Zhou,[‡] and Hai-Feng Ji*[,†]

[†]Department of Chemistry, Drexel University, 32 South 32nd Street, Philadelphia Pennsylvania 19104, United States

[‡]Department of Mechanical Engineering and Mechanics, Drexel University, 3141 Chestnut Street, Philadelphia Pennsylvania 19104, United States

Supporting Information

ABSTRACT: 4D printing is an emerging additive manufacturing technology that combines the precision of 3D printing with the versatility of smart materials. 4D printed objects can change their shape over time with the application of a stimulus (i.e., heat, light, moisture). Light driven smart materials are attractive because light is wireless, remote, and can induce a rapid shape change. Herein, we present a method for fabricating polymeric bilayer actuators via 3D printing which reversibly change their shape upon exposure to light. The photoactive layer consists of a poly(siloxane) containing pendant azobenzene groups. Two different photoactive polymers were synthesized, and the photomechanical effect displayed by the bilayers was evaluated. These bilayers exhibit rapid actuation with full cycles completed within seconds, and photo generated stresses ranging from 1.03 to 1.70 MPa.

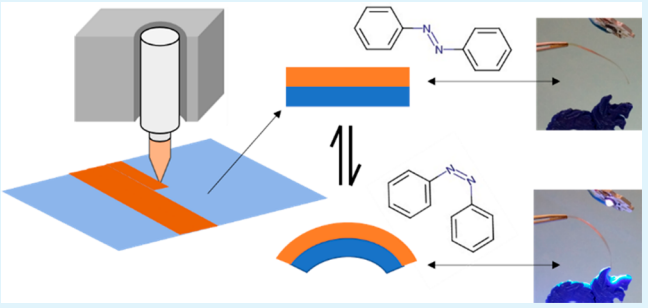

KEYWORDS: *3D printing; azobenzene, poly(siloxanes), smart materials, photoactivated, bilayer*

INTRODUCTION

The incorporation of smart materials into a three-dimensional (3D) printed object that enable its reversible transformation (e.g., shape) in response to an external stimulus is referred to as 4D-printing. This technique was recently developed by Tibbits et al.[1,2] They fabricated objects comprised of a hydrogel and rigid plastic. When immersed in water, the hydrogel swells while the plastic is unaffected. With the aid of 3D-modeling and precise placement of both components, the expanding hydrogel causes the object to change its shape. They created 4D-printed objects capable of 1D to 2D, 1D to 3D, and 2D to 3D transitions via bending and folding motions.[3] With their technique, the hydrogel serves as the active material, while the plastic is a passive component, and the stimulus is water.

Ge et al. developed a different 4D printing technique which relies on printed active composites (PACs) to enable a shape-change in their objects.[4] PACs consist of glassy polymer fibers embedded in an elastomeric matrix. The glassy polymer fibers exhibit the shape-memory effect. The shape-change is achieved by the standard thermomechanical programming steps for shape memory materials. The original shape is recovered by heating the PAC above its glass transition temperature (T_g). PACs are capable of bending, twisting, and curling motions by adjusting the fiber orientation. These PACs were also incorporated into larger 4D-printed objects. Six rigid plastic panels were connected by PAC hinges to demonstrate a 2D to 3D shape change. By using the thermomechanical programming steps mentioned above, the initial 2D object was transformed into a cube.[5] In this example, the PAC is the active material, the rigid panels are the passive component, and the stimulus is the combination of heat and mechanical stress.

Since their work, there have been many examples of multimaterial 3D-printing being implemented to produce 4D printed objects for various applications.[6−10] A recent review covers the 4D-printing process and shape-changing mechanisms of 4D-printed objects comprehensively.[11] Out of the many examples of 4D-printed objects to date, most rely on the swelling of hydrogels or shape-memory effects to cause a shape change. Using light as the stimulus for a 4D-printed object would be an attractive alternative because light is remote, wireless, spatially precise, and sources of various wavelengths and intensities are readily available. Photoresponsive liquid crystal elastomers (LCEs) are a well-known class of materials that can reversibly change their shape when stimulated with light.[12−15] They are comprised of a cross-linked polymeric network which includes photosensitive liquid crystalline (LC) mesogens that can be located in the main chain of the polymer or attached to the polymer backbone as a side group.[16−19] Common photosensitive molecules in these LCEs are azobenzene (AB) derivatives. The trans isomer of AB is a rod-shaped molecule while the cis isomer is bent. Irradiation with the appropriate wavelength causes AB to undergo a trans−cis isomerization. In LCEs this isomerization induces a

Received: May 22, 2018
Accepted: July 23, 2018
Published: July 23, 2018

DOI: 10.1021/acsami.8b08503
ACS Appl. Mater. Interfaces 2018, 10, 27308−27315

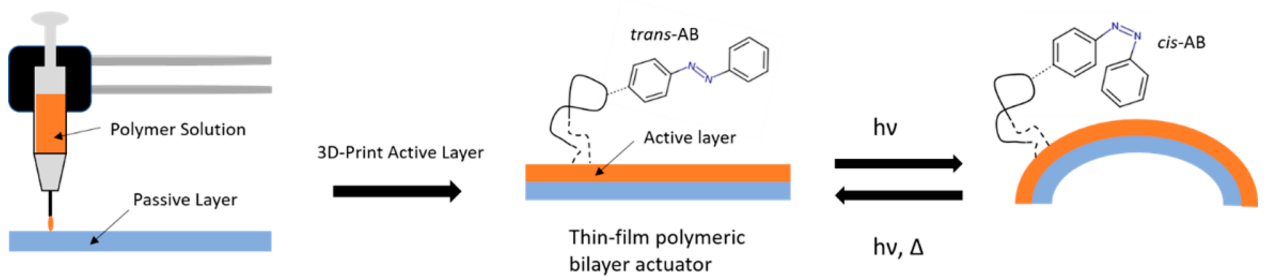

Figure 1. Fabrication of a photoactive, flexible thin-film bilayer actuator via 3D-printing.

phase change from an initially ordered LC phase to a disordered isotropic phase, which causes a contraction in the same direction as the LC director. The original shape can be recovered by switching AB from the cis isomer back to the trans isomer by either thermal relaxation or irradiating the LCE with the appropriate wavelength of light. Alignment of LC mesogens is achieved in monodomain LCEs by mechanically stretching partially cross-linked thin films while performing a second cross-linking step to fully cure the samples.[20] Another method of LC alignment is the use of command surfaces in contact with the reaction mixture during the synthesis of LCE thin films.[21−23] These alignment techniques present challenges when trying to use additive manufacturing to print stimuli responsive LCE objects. Research efforts in this area recently demonstrated that shear forces generated from extruding viscous LCE precursor ink could be used for LC alignment while 3D printing thermotropic LCE objects, although the LCE ink must possess specific rheological properties to achieve LC alignment during printing.[24,25]

Herein, we present a simple method for 3D printing polymeric bilayer actuators (Figure 1) that require only light input to achieve a reversible shape change. One layer consists of a photoactive poly(siloxane) containing pendant azobenzene groups, which we refer to as the active layer. LCEs that consist of poly(siloxane)s containing photoswitchable groups have been extensively studied, but these materials consist of cross-linked polymers.[26] By omitting the cross-linking step we obtain linear polymers to use in the active layer which are soluble in common organic solvents (e.g., toluene) and therefore can be printed from solution via syringe 3D printing. The second layer, which we refer to as the passive layer, is comprised of commercially available Kapton polyimide thin films. We used polyimide thin films to serve as the passive layer since they are flexible, inert to most organic solvents, and have desirable mechanical properties. The bilayers are fabricated in one step by printing directly onto the passive layer which has been precut into the desired shape and fixed to the print bed.

Irradiating the bilayers with the appropriate wavelength light causes a trans−cis isomerization of the AB molecules in the active layer. Due to the size difference of the AB isomers, the isomerization requires a free volume increase of the polymer matrix, which results in an overall volume expansion of the active layer.[27] Under the correct conditions, this photoinduced volume expansion creates a strain gradient between the active and passive layers large enough to deform the bilayer. This shape change is reversible because when the light source is turned off, the AB molecules undergo the cis−trans isomerization, returning the deformed bilayer to its original shape. In these bilayers, the shape-change relies on the volume change of the active layer, not the alignment of the AB molecules within a cross-linked polymer network as is the case for LCEs. While the overall volume change of the active layer is small,[27,28] it can be amplified into large deformations using a bilayer actuator configuration.[29,30] Also, we do not cross-link the polymers in the active layer so we can use relatively simple and inexpensive 3D printers when compared with the multimaterial 3D printers commonly used to make stimuli responsive objects. We synthesized two different light responsive polymers to serve as the active layer and compared the behavior of the resultant bilayer actuators to explore this method.

EXPERIMENTAL SECTION

Materials. Polymethylhydrosiloxane (PHMS) with molecular weight (MW) 2100−2400 g/mol was purchased from Gelest, Inc. Dihydrogen hexachloroplatinate (IV) hydrate (H_2PtCl_6, 99.9% metals basis) was purchased from Alfa Aesar. 6-bromo-1-hexene was purchased from Oakwood Chemical. Toluene (Fisher Chemical) was freshly distilled from Na/Benzophenone ketyl prior to use. Anhydrous dimethylacetamide (DMAC) was purchased from Alfa Aesar and stored over 4 Å molecular sieves. All other chemicals were purchased from either Sigma-Aldrich or Alfa Aesar and used without further purification. Kapton Type 100 HN nonadhesive sheets were obtained from Cole Palmer. Light emitting diodes (LED) used were ultramarine royal blue LED (440−445 nm), CREE XP-E green LED (535 nm) purchased from Rapidled, and a high-power single-color UV LED (LED Engin) (365 nm) purchased from Mouser Electronics.

(E)-[4-(hex-5-en-1-yloxy)phenyl](4-methoxyphenyl)diazene (M1). 4-Methoxy-4′-hydroxyazobenzene (12 g, 52.6 mmol) was dissolved in approximately 70 mL of DMAC. Potassium carbonate (10.9 g, 78.9 mmol) was added in one portion with stirring. The reaction mixture was heated to 95 °C. After 30 min, 6-bromo-1-hexene (8.6 g, 52.6 mmol) was added dropwise. The reaction was kept at 95 °C under an atmosphere of nitrogen overnight. The reaction mixture was cooled to room temperature and then poured into ice-cold water. The precipitate was collected by vacuum filtration and was washed with water until the washings were neutral to pH paper. This crude product was recrystallized in 95% (v/v) ethanol to give gold colored plates, then dried at 60 °C under vacuum to yield 13.8 g (85%) of M1. ^{1}H NMR (500 MHz, $CDCl_3$) δ: 7.90−7.85 (4H, m), 7.03−6.97 (4H, m), 5.85 (1H, ddt, J = 17, J = 10, J = 7), 5.14−4.97 (2H, m), 4.05 (2H, t, J = 6), 3.89 (3H, s), 2.16 (2H, q, J = 7), 1.85 (2H, quint, J = 7), 1.60 (2H, quint, J = 8) (Supporting Information (SI) Figure S3). HR-MS (APCI): m/z calcd. for $C_{19}H_{23}O_2N_2$ ($[M + H]^+$): 311.1754, found: 311.1757.

N-ethyl-N-[2-(hex-5-en-1-yloxy)ethyl]-4-[(E)-2-(4-nitrophenyl)-diazen-1-yl]aniline (M2). 18-crown-6 (420 mg, 1.6 mmol) and finely ground potassium hydroxide (4.46g, 80 mmol) were added to 40 mL of tetrahydrofuran. Disperse red 1 (5.0 g, 16 mmol) was added to the reaction in one portion with stirring. A solution of 6-bromo-1-hexene (3.26 g, 20 mmol) in 10 mL of tetrahydrofuran was then added dropwise. The reaction was stirred at 30 °C for 16 h. The volume of tetrahydrofuran was reduced to approximately 20 mL on a rotary evaporator. The reaction mixture was diluted with 100 mL of DI water and transferred to a separatory funnel. The product was extracted into dichloromethane, the solution dried with anhydrous sodium sulfate, filtered, and the solvent removed on the rotary

DOI: 10.1021/acsami.8b08503
ACS Appl. Mater. Interfaces 2018, 10, 27308−27315

evaporator. The residue was purified by column chromatography using hexanes/ethyl acetate (5:1 v/v) to give 3.91 g of M2 as a red solid in 62% yield. ^{1}H NMR (500 MHz, $CDCl_3$) δ: 8.23 (2H, d, J = 9), 7.85−7.79 (4H, m), 6.69 (2H, d, J = 9), 5.71 (1H, ddt, J = 17, J = 10, J = 7), 4.92 (1H, d, J = 17), 4.87 (1H, d, J = 10), 3.56−3.53 (4H, m), 3.47 (2H, q, J = 7), 3.38 (2H, t, J = 7), 1.99 (2H, q, J = 7), 1.51 (2H, quint, J = 7), 1.37 (2H, quint, J = 8), 1.17 (3H, t, J = 7) (SI Figure S4). HR-MS (APCI): m/z calcd. for $C_{22}H_{29}O_3N_4$ ($[M + H]^+$): 397.2234, found: 397.2232.

Polymethylhydrosiloxane-g-(4-methoxy-4′-hexyloxyazobenzene) (P1). A Teflon stir bar and M1 (8.0 g, 26 mmol) were added to a flame-dried 250 mL round-bottomed flask which was transferred to a glovebox under a nitrogen atmosphere. To the flask was added chloroplatinic acid (10.6 mg, 26 μmol), PHMS (1.65g), and approximately 130 mL of toluene. The flask was sealed with a rubber septum and transferred to a fume hood where it was heated to 100 °C under nitrogen for 24 h. The reaction was cooled to room temperature and precipitated into 1 L of hexane. The crude polymer product was collected by filtration. The polymer was then purified by repeated dissolution in a minimum volume of dichloromethane and precipitation into hexanes until no trace of M1 was detected by thin layer chromatography (TLC). Yield of P1 was 7.15 g (74%) of a yellow-green powder. ^{1}H NMR (500 MHz, $CDCl_3$) δ: 7.75 (4H, s), 6.85 (4H, s), 4.70 (1H, s), 3.80 (5H, m), 1.68 (2H, s), 1.35 (6H, m), 0.51 (2H, s), 0.15 (3H, s), 0.06 (3H, s) (SI Figure S5).

Polymethylhydrosiloxane-g-N-ethyl-N-[2-(hexyloxy)ethyl]-4-[2-(4-nitrophenyl)diazen-1-yl]aniline (P2). A Teflon stir bar and M2 (3.69 g, 9.3 mmol) were added to a flame-dried 100 mL round-bottomed flask and transferred to a glovebox containing a nitrogen atmosphere. To the flask was added chloroplatinic acid (3.8 mg, 9.3 μmol), PHMS (598 mg), and approximately 35 mL of toluene. The flask was sealed with a rubber septum and transferred to a fume hood where it was heated to 100 °C under nitrogen for 24 h. The reaction was cooled to room temperature. The reaction contained a small amount of insoluble material which was filtered off prior to precipitation into 300 mL of cold hexanes. The crude polymer product was collected by filtration on a glass fritted funnel. The polymer was then purified by repeated dissolution in a minimum volume of dichloromethane and precipitation into hexanes until no trace of M2 was detected by TLC. Yield of P2 was 1.97 g (46%) of a dark red solid. ^{1}H NMR (500 MHz, $CDCl_3$) δ: 8.17 (2H, s), 7.76 (4H, s), 6.62 (2H, s), 4.17 (1H, s), 3.40 (8H, m), 1.48 (2H, s), 1.24 (6H, m), 1.11 (3H, s), 0.44 (2H, s), 0.04 (6H, m) (SI Figure S6).

3D-Printing. A solution of either P1 or P2 (8−10% w/w in toluene) was loaded into the syringe. The syringes and dispensing nozzle (25 gauge) were made of polypropylene (McMaster Carr). The printer speed was set to 200 mm/min and the height of the printer nozzle was adjusted manually at 0.25 mm above the Kapton film. The printer nozzle and substrate were set to room temperature of 25 °C. A simple rectangle measuring at 6.20 mm in length and 20 mm in width was designed in Creo Paramtric 3.0, converted into G-code, and uploaded to the 3D printer for the 3D printing of the bilayers. During printing, the nozzle moves in a rectilinear motion on a line-by-line basis to create a homogeneous layer of either P1 or P2 on top of the Kapton substrate (SI Movie S1).

Instrumentation. An Agilent 8453 spectrophotometer equipped with a diode array detector was used to collect the UV−vis spectra. Samples were prepared by spin-coating (SCS 6800 series) thin films of P1 or P2 onto precleaned quartz slides from a 1% (w/w) solution in THF. Differential scanning calorimetry (DSC) was performed on a TA Q-100 series instrument using aluminum sample pans (DSC Consumables, Inc.). ^{1}H nuclear magnetic resonance (NMR) spectra were collected on a 500 MHz Varian INNOVA spectrometer in deuterated chloroform (Cambridge Isotopes Laboratory). The spectra were either referenced to the residual chloroform signal (7.26 ppm) or a tetramethylsilane (TMS) internal standard (0.00 ppm). Photogenerated stress was measured using a TA Instruments model 2980 dynamic mechanical analyzer (DMA). Measurements were taken in constant strain mode using an oscillation amplitude of 50 μm and constant static force of 40 mN. A 3D bioprinter, Tissue Scribe, from 3D Cultures was used to perform 3D printing. Light intensities were measured using a Newport model 1916-C optical power meter.

RESULTS AND DISCUSSION

To realize our 3D printed light activated bilayer actuator, we first synthesized linear poly(siloxane)s containing pendant azobenzene groups (Scheme 1) to serve as the active layer.

Scheme 1. Reaction Scheme Employed to Synthesize Shape-Changing Polymers P1 and P2

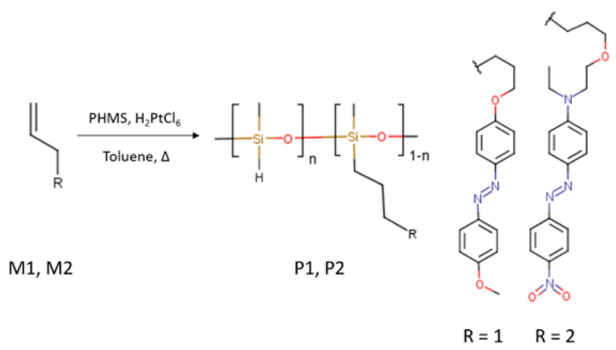

The general strategy we employed covalently attached an AB molecule containing a terminal double bond to the Si−H functional groups of poly(hydrogen methyl siloxane) (PHMS) using a platinum catalyzed hydrosilylation reaction. This results in a random distribution of AB grafted to the poly(siloxane) backbone. Polymethylhydrosiloxane-*g*-(4-methoxy-4′-hexyloxyazobenzene) (P1) has pendant AB groups which are substituted at the 4 and 4′ positions with alkoxy functional groups. The synthesis of P1 proceeds smoothly using the given reaction conditions, with polymer yields reaching 74%. ^{1}H NMR was employed to estimate the amount of AB grafted to the PHMS backbone by integrating the residual Si−H proton and one of the aromatic signals of AB. From the ratio of the two integrals we calculated the average grafting density of AB to be 0.84 for P1.

Polymethylhydrosiloxane-*g*-*N*-ethyl-*N*-[2-(hexyloxy)ethyl]-4-[2-(4-nitrophenyl)diazen-1-yl]aniline (P2) contains a push−pull type pendant AB group. AB substituted with strong electron withdrawing groups (e.g., nitro) and strong electron donating groups (e.g., dialkylamino) at the 4 and 4′ positions are referred to as push−pull ABs. Relative to AB, the $\pi-\pi^*$ transition for push−pull ABs is lower in energy which shifts it into the visible region of the spectrum and causes it to overlap with the $n-\pi^*$ transition.[31] They also exhibit very fast thermal cis−trans thermal isomerization rates which can be completed in milliseconds, depending on the chemical environment.[32] The push−pull AB pendant group in P2 is a derivative of the well-known disperse red 1 (DR1) AB dye. We chose to incorporate this AB molecule into P2 for several reasons. The shape change of a bilayer actuator is proportional to the volume change of active layer. Push−pull AB photoisomerization can proceed through rotation rather than inversion, which inherently requires greater free volume to occur. The nonpolar poly(siloxane) backbone is covalently bound to a highly polar AB molecule which could result in unique properties compared to the relatively nonpolar AB molecule in P1. Also, as mentioned above the fast thermal cis−trans isomerization could increase the rate at which the actuators can by cycled. The synthesis of P2 has not been reported in the literature to

DOI: 10.1021/acsami.8b08503
ACS Appl. Mater. Interfaces 2018, 10, 27308−27315

the best of our knowledge, making it a novel photoactive polymer. The synthesis of P2 was carried out using the same reaction conditions as for P1. The grafting density of P2, measured in the same way as described earlier, was calculated to be 0.68. The grafting density of P2 is comparable to that of P1, but the overall polymer yields from the reaction were lower, ranging from 30 to 46%. This is most likely due to poisoning of the platinum catalyst, as similar yields have been reported for hydrosilylation reactions involving aminated alkenes.[33] Following the synthesis of the active layer materials P1 and P2, bilayers were fabricated using a 3D-printer (Tissue Scribe) capable of depositing the polymers from solution onto the passive layer by extrusion through a syringe. We printed the P1/Kapton and P2/Kapton bilayers using an 8% (w/w) solution in toluene. This produced P1 film thicknesses of 8 ± 1 μm on average (SI Figure S1). The solution of P2 in toluene was more viscous and using the same 3D printing settings resulted in film thicknesses of 30 ± 2 μm on average (SI Figure S2).

Differential scanning calorimetry (DSC) was employed to investigate the thermal properties of P1 and P2. The DSC traces for P1 and P2 are shown in Figures 2 and 3, respectively.

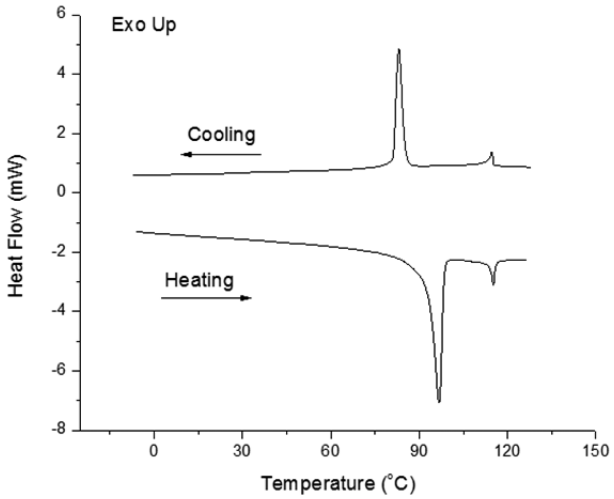

Figure 2. DSC heating and cooling traces of P1. The heating and cooling rates were 10 °C per minute and 5 °C per minute, respectively.

The heating scan of P1 reveals two sharp transitions at 97 and 115 °C. Being a semicrystalline polymer, the peak at 97 °C is the crystalline to LC transition, and the peak at 115 °C is a LC to isotropic transition. No other peaks were observed for P1 in both heating and cooling scans which is one indication the LC phase is nematic. Quench cooling revealed an otherwise difficult to detect T_g for P1 which was determined to be approximately 26 °C. During the second heating scan, P2 exhibits one broad endothermic event. This peak was attributed to melting of the polymer, with an onset temperature of 60 °C. Upon cooling, there are two small and broad overlapped peaks centered at 78 and 72 °C, followed by a large exothermic event with an onset temperature at 51 °C. The heterogeneous nature of the P2 polymer chains could cause it to crystallize over a relatively long period of time. The initial exothermic peaks could indicate the formation of small crystallites, followed by further crystallization of the sample upon continued cooling. From

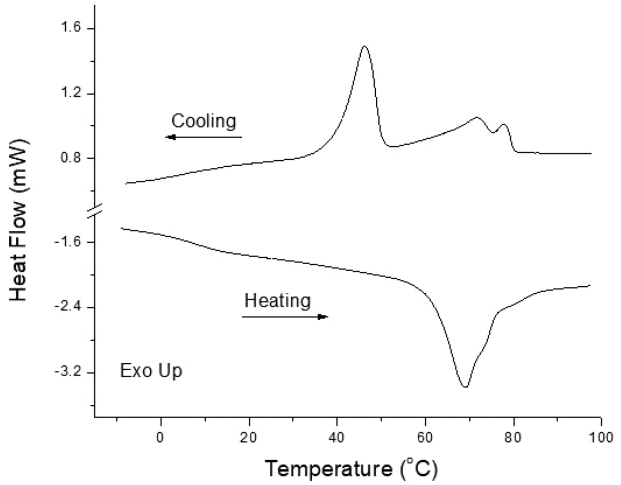

Figure 3. DSC heating and cooling traces of P2. The heating and cooling rates were 10 °C per minute and 5 °C per minute, respectively.

DSC alone, it is unclear if P2 has an LC phase. For P2, the T_g can be seen in both heating and cooling scans and was found at 8 °C, reported as the midpoint of the transition. Poly(siloxane)s can have relatively low T_g values due to the flexibility of the Si−O linkages in the polymer chains and is one reason they were chosen.[34] In LCEs possessing T_g values well above room temperature, multiple stimuli are needed because light alone is insufficient to heat them above their T_g.[13,16] With P1 and P2 having T_g near or below room temperature, our bilayers only need light input to change their shape. This design aspect is beneficial because using a single stimulus simplifies the shape change process for these objects.

UV−vis spectroscopy was used to study the optical properties of the synthesized polymers, as well as the isomerization behavior of the AB moieties grafted to the siloxane backbone. A comparison between the UV−vis spectra of P1 and P2 are shown in Figure 4. The absorption spectrum of P1 shows the $\pi-\pi^*$ transition for the trans isomer appears at λ = 355 nm while the $n-\pi^*$ transition of the trans isomer appears as a weak shoulder at λ = 450 nm. Overlap of these two main transitions is common for ABs containing amino,

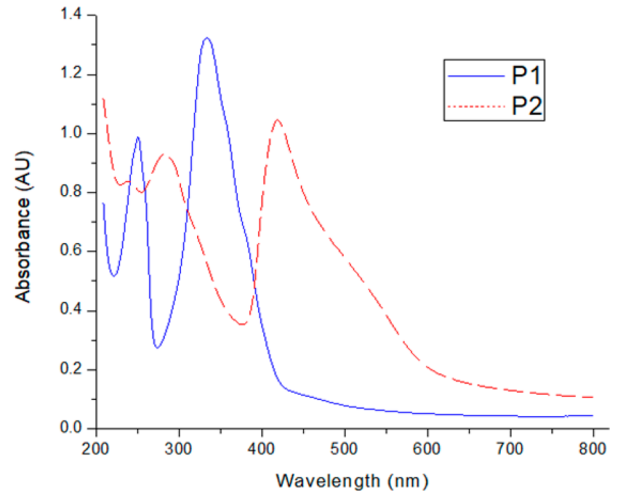

Figure 4. UV−vis spectra of thin films of P1 and P2 deposited onto quartz slides.

DOI: 10.1021/acsami.8b08503
ACS Appl. Mater. Interfaces 2018, 10, 27308−27315

hydroxyl, or alkoxy substituents at the four positions.[35] Relative to azobenzene, both the $\pi-\pi^*$ and $n-\pi^*$ transitions of the AB mesogen in P2 are shifted toward higher wavelengths.[36] P2 exhibits an absorption band at λ = 420 nm ($\pi-\pi^*$) with a broad shoulder centered at λ = 530 nm. The band at 420 nm in Figure 4 is strongly blue-shifted (~63 nm) compared to the absorption spectrum of P2 dissolved in dichloromethane, a nonpolar solvent (SI Figure S7). The absorption spectrum of P2 in dichloromethane has only one broad peak in the visible range with the maximum absorbance located at λ = 483 nm. A blue-shift of this magnitude observed for P2 thin films could be attributed to H-aggregates of the AB moieties in the thin film.[37] The absorbance at 530 nm is too high to be from only the $n-\pi^*$ transition since it is a symmetry forbidden transition. The absorbance at this wavelength is likely from the $n-\pi^*$ of the AB groups and the $\pi-\pi^*$ transition of AB molecules in P2 which are not aggregated but interact mostly with the polymer matrix. This behavior is a consequence of the synthetic strategy we employed, which grafts AB randomly to the polymer backbone.

Figures 5 and 6 show the isomerization behavior of thin films of P1 and P2, respectively. For P1, the irradiation with

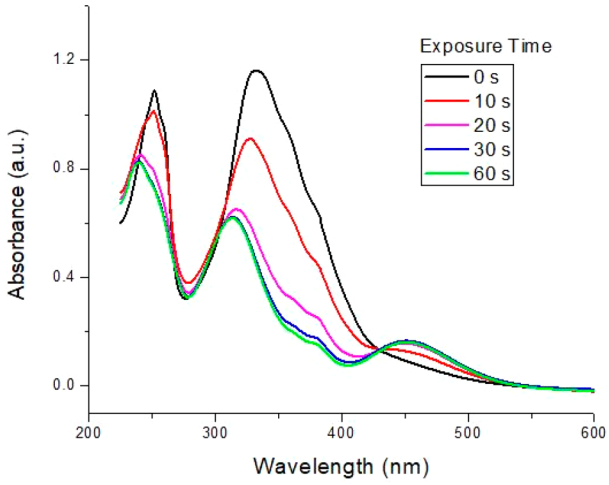

Figure 5. UV−vis spectra of a thin film of P1 during exposure to 365 nm wavelength light.

UV light induces the trans−cis isomerization. As seen in Figure 5, the spectral changes stopped after 30 seconds indicating a photostationary state was reached. The spectra show the usual decrease in absorbance of the band at λ = 355 nm and an increase of absorbance from the band at λ = 450 nm which is due to the enrichment of the cis isomer in the thin film. The trans isomer was recovered by irradiating the sample with a LED emitting green light (535 nm) (SI Figure S8) within 60 seconds. The trans isomer was completely recovered with no apparent fatigue or bleaching of the AB moiety.

The absorption spectra of a P2 thin film irradiated with a 442 nm LED are shown in Figure 6. Irradiation with a blue light LED (442 nm) caused the trans−cis isomerization of AB groups in P2. This was confirmed by a decrease in the absorbance of the band at λ = 420 nm and an increase at λ = 530 nm. P2 contains push−pull type AB pendant groups, which exhibit fast thermal cis−trans isomerization, one reason such a small change in absorbance is observed for the photostationary state. Similar results have been reported on

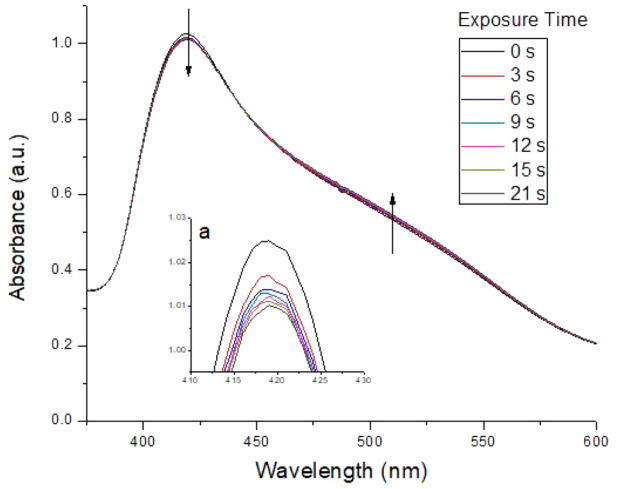

Figure 6. UV−vis spectra of a thin film of P2 during exposure to 442 nm wavelength light. The inset (a) shows a magnified view of the absorption band located at λ = 420 nm.

photoisomerization studies of DR1 in solution[38] and in DR1 functionalized poly(methyl methacrylate) thin films.[39]

The photomechanical effect exhibited by these actuators was investigated by recording videos of the P1/Kapton and P2/Kapton bilayers when exposed to 365 or 442 nm wavelength LEDs. Rectangular bilayers were made according to the steps portrayed in Figure 1. Still images from a test of a P1/Kapton bilayer using a UV LED are shown in Figure 7. The bending of

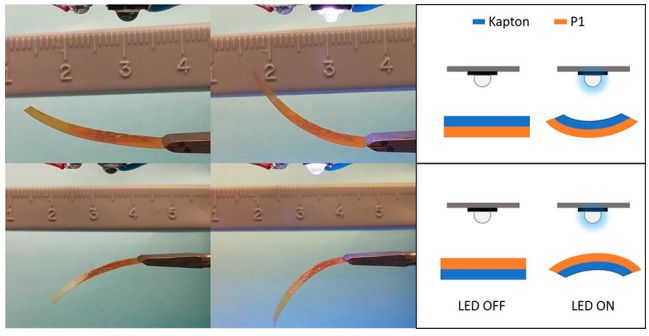

Figure 7. Images of a P1/Kapton bilayer fixed at one end when the UV LED is OFF (left) and the UV LED is ON (right). The scale in the background is in centimeters, and the light intensity is about 80 mW/cm^2.

a P1/Kapton bilayer using a blue-light LED is depicted in SI Figure S12. When either LED light source was placed above the active layer of the P1/Kapton bilayer and switched on, the actuator immediately bent away from the light source (SI Movie S2). If the bilayer was flipped over and the bending test was performed in the opposite geometry, with light traveling through the passive layer first, the P1/Kapton bilayer bends toward the light source. Depending on the placement of the light source the bilayers either bend toward or away from it, but the bilayers always transform into the same shape. This behavior is observed for both LEDs and for the P2/Kapton bilayers (not shown) as well. The maximum bending angle for the P1/Kapton bilayer achieved with either light source was thirty-five degrees. The light intensities needed to induce this actuation were approximately 150 mW/cm^2 and 100 mW/cm^2 for the UV and blue LEDs, respectively. Larger bending angles

DOI: 10.1021/acsami.8b08503
ACS Appl. Mater. Interfaces 2018, 10, 27308−27315

were not observed by further increasing the light intensities (up to 300 mW/cm^2). Within five seconds of either light source being turned on, the P1/Kapton bilayer was able to reach the maximum bending angle. When the LED was switched off, it took about 10 seconds for the actuator to return to its original position. To see if there is any fatigue of the active layer, the actuation cycle was repeated multiple times and the deflection angle was monitored. After 10 cycles the actuator showed no fatigue, and for each cycle it reached the maximum deflection angle of thirty-five degrees (SI Figure S9).

For P2/Kapton bilayers, both the UV and blue LEDs caused rapid bending when the light sources were turned on. When bending tests were performed with blue LEDs (SI Figure S10) the maximum bending angle of 14 degrees was reached within two seconds. Then, while the light source was still on, the actuator bending angle rapidly decreased to a value between six and eight degrees. This secondary bending angle was stable while the LED was on (SI Movie S3). When the LED was turned off, the actuator returned to its original position in approximately ten seconds. This behavior could be explained by the trans−cis−trans cycling of the AB mesogen in P2 when irradiated with blue-green light. Initially the rapid trans−cis isomerization in the active layer results in a volume increase proportional to the maximum displacement observed for the P2/Kapton bilayer, then trans−cis−trans cycling allows the P2 molecules to reorganize which is accompanied by a decrease in volume and subsequent decrease in bending angle. When the P2/Kapton bilayers were irradiated with the UV LED, the bending angle stayed relatively constant while the light was on. The average bending angle observed over five trials was 13 degrees. This was comparable to the maximum bending angles recorded when testing P2/Kapton bilayers with the blue-light LED.

The photogenerated stress of the bilayers and blank Kapton films were measured using DMA. Samples were precut into rectangles measuring 30 × 7.5 mm in length and width, respectively. They were clamped in tension longitudinally at both ends. The light sources were placed 10 mm away from the surface of the film samples. For the P1/Kapton and P2/Kapton bilayers, the active layer was always facing the light source. Figure 8 shows that when irradiated with 442 nm light (225 mW/cm^2), there was an immediate decrease in stress for all three samples. The first time the samples were irradiated, the stress relaxed to 80−85% of the initial stress value for all three samples. The stress reached a constant value after the light was turned off within 20 s for Kapton and P1/Kapton bilayer, whereas it took the P2/Kapton bilayer 80 s to relax. Over the next three on/off cycles when the light was turned off, the stress relaxed to 98−100% of the initial stress value before irradiation. The time it took the samples to relax remained constant. From several on/off cycles, the average change in stress was estimated to be 550 kPa for Kapton, 1025 kPa for the P1/Kapton bilayer, and 1425 kPa for the P2/Kapton bilayer. The decrease in stress is caused by an expansion of the samples along its vertical axis.[40,41] The change in stress for the bare Kapton is likely a thermal effect due to absorption of light used to irradiate the samples. Since both P1 and P2 polymers strongly absorb light in the UV−vis region, this thermal effect observed for bare Kapton would be decreased for the P1/Kapton and P2/Kapton bilayers in our experimental setup. Even when correcting for this effect, both bilayers exhibit a larger change in stress than observed for the bare Kapton samples which indicates that the photoactive layer

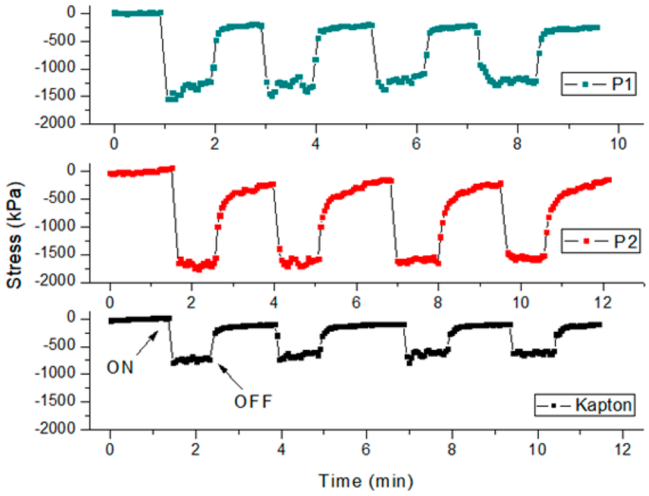

Figure 8. Change in stress from DMA measurements of bare Kapton as well as P1/Kapton and P2/Kapton bilayers when irradiated with 442 nm wavelength light. The light intensity of the LED was 225 mW/cm^2.

does create a stress gradient in the bilayers when irradiated with either UV or blue light.

Figure 9 shows the change in stress for a bare Kapton thin film, a P1/Kapton bilayer, and P2/Kapton bilayer when

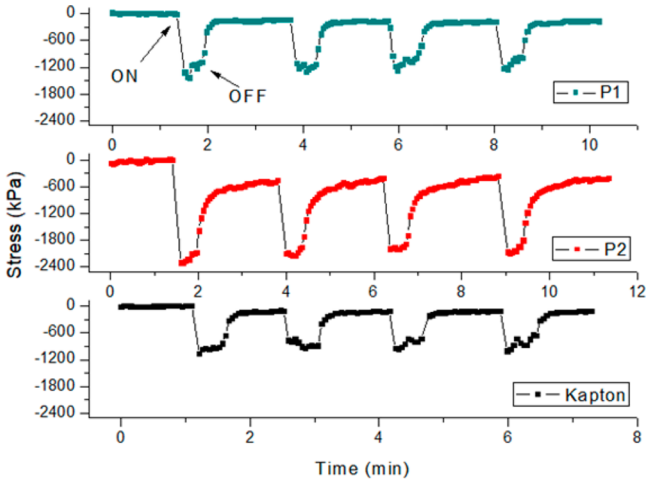

Figure 9. Change in stress from DMA measurements of bare Kapton as well as P1/Kapton and P2/Kapton bilayers when irradiated with 365 nm wavelength light. The light intensity of LED was 220 mW/cm^2.

irradiated with UV light (220 mW/cm^2). The average change in stress was about 775 kPa for bare Kapton, 1100 kPa for the P1/Kapton bilayer, and 1700 kPa for the P2/Kapton bilayer. For all three samples the average change in stress was slightly higher than when the 442 nm LED was used. This observation is likely due to a slight difference in temperature of the measured samples because the heat caused by the absorption of light will vary when using the 365 nm or the 442 nm light source. The photogenerated stress measured for the P1/Kapton and P2/Kapton using either light source is on the same order of magnitude reported for LCE samples (0.37−2.6 MPa).[41] The change in stress measured for the P2/Kapton bilayers was larger than the P1/Kapton bilayers regardless of the light source used, but the P1/Kapton bilayers out-

DOI: 10.1021/acsami.8b08503
ACS Appl. Mater. Interfaces 2018, 10, 27308−27315

performed the P2/Kapton bilayers in the bending tests. The actuation of the bilayers depends on multiple factors including strain, Young's modulus, and thicknesses of the active and passive layers. A T_g well below room temperature and the results of the bending tests suggest that P2 lacks the mechanical properties to convert the photogenerated stress into a strain gradient as effectively as P1. Stiffening the pendant AB groups by shortening the alkyl spacer between the polymer backbone could be one way to improve the mechanical properties of P2. When compared to P1, it is unclear if the larger photogenerated stress for P2 is due to the higher flexibility of the polymer[42] or the nature of the photoisomerization of push−pull ABs.

CONCLUSIONS

Two side-chain AB poly(siloxane)s, one being reported for the first time, were synthesized to serve as the photoactive layer of bilayer actuators fabricated via 3D-printing. The reversible shape-change these objects exhibited was rapid, with actuation cycles completed on the time scale of seconds. UV−vis spectroscopy and DMA measurements confirm that the trans−cis isomerization of AB in the active layer generated the stress responsible for the shape changes observed in the bilayers. The P2/Kapton bilayer exhibited the largest amount of light induced stress, however larger bending angles were observed for the P1/Kapton bilayers. While push−pull type AB show promise as pendant groups for these photoactive polymers, more research could increase their efficiency in converting photogenerated stress to mechanical work. For P2, shortening the alkyl spacer between the AB mesogen and the poly(siloxane) backbone and/or increasing the AB grafting density could lead to such improvements. Research in this area is ongoing as well as fabricating more versatile shape-changing objects.

ASSOCIATED CONTENT

Supporting Information

The Supporting Information is available free of charge on the ACS Publications website at DOI: 10.1021/acsami.8b08503.

Video of P2/Kapton bilayer being 3D-printed (Movie S1) (MPG)

Video of P1/Kapton bilayer actuation (Movie S2) (MPG)

Video of P2/Kapton bilayer actuation (Movie S3) (MPG)

SEM images of P1/Kapton and P2/Kapton bilayer cross sections (Figures S1, S2), ^{1}H NMR spectra of synthesized compounds M1, M2, P1, and P2 (Figures S3−S6), UV−vis spectrum of P2 in solution (Figure S7), cis−trans photoisomerization measurement of P1 with green-light LED (Figure S8), Plots of bending angle vs time for P1/Kapton and P2/Kapton bilayers (Figures S9, S10), Plots of bending angle vs time and displacement vs time for P1/Kapton bilayers (Figure S11), Bending images of a P1/Kapton bilayer exposed to a blue-light LED (Figure S12) (PDF)

AUTHOR INFORMATION

Corresponding Author

*Phone: 01-215-895-2562. Fax: 01-215-895-1265. E-mail: hj56@drexel.edu.

ORCID

Hai-Feng Ji: 0000-0001-5450-0121

Notes

The authors declare no competing financial interest.

ACKNOWLEDGMENTS

This work was supported by NSF CMMI- 1538318. We would like to thank Dr. Palmese and John Vergara from the Chemical and Biological Engineering Department at Drexel University for their help with the dynamic mechanical analysis measurements.

REFERENCES

(1) Tibbits, S. The Emergence of "4D Printing. In *TED Conference*, 2013.

(2) Tibbits, S. 4D Printing: Multi-Material Shape Change. *Archit. Des.* **2014**, *84* (1), 116−121.

(3) Tibbits, S.; McKnelly, C.; Olguin, C.; Dikovsky, D.; Hirsch, S. *4D Printing and Universal Transformation*; ACADIA, 2014.

(4) Ge, Q.; Qi, H. J.; Dunn, M. L. Active Materials by Four-Dimension Printing. *Appl. Phys. Lett.* **2013**, *103* (13), 131901.

(5) Ge, Q.; Dunn, C. K.; Qi, H. J.; Dunn, M. L. Active Origami by 4D Printing. *Smart Mater. Struct.* 2014, *23* (9).

(6) Sydney Gladman, A.; Matsumoto, E. A.; Nuzzo, R. G.; Mahadevan, L.; Lewis, J. A. Biomimetic 4D Printing. *Nat. Mater.* **2016**, *15* (4), 413−418.

(7) Ge, Q.; Sakhaei, A. H.; Lee, H.; Dunn, C. K.; Fang, N. X.; Dunn, M. L. Multimaterial 4D Printing with Tailorable Shape Memory Polymers. *Sci. Rep.* **2016**, *6* (April), 1−11.

(8) Zhang, Q.; Zhang, K.; Hu, G. Smart Three-Dimensional Lightweight Structure Triggered from a Thin Composite Sheet via 3D Printing Technique. *Sci. Rep.* **2016**, *6* (1), 22431.

(9) Li, H.; Gao, X.; Luo, Y. Multi-Shape Memory Polymers Achieved by the Spatio-Assembly of 3D Printable Thermoplastic Building Blocks. *Soft Matter* **2016**, *12* (13), 3226−3233.

(10) Wei, H.; Zhang, Q.; Yao, Y.; Liu, L.; Liu, Y.; Leng, J. Direct-Write Fabrication of 4D Active Shape-Changing Structures Based on a Shape Memory Polymer and Its Nanocomposite. *ACS Appl. Mater. Interfaces* **2017**, *9* (1), 876−883.

(11) Momeni, F.; Mehdi, M.; Hassani, N. S.; Liu, X.; Ni, J. A Review of 4D Printing. *Mater. Des.* **2017**, *122*, 42−79.

(12) Finkelmann, H.; Nishikawa, E.; Pereira, G. G.; Warner, M. A New Opto-Mechanical Effect in Solids. *Phys. Rev. Lett.* **2001**, *87* (1), 1−4.

(13) Yu, Y.; Nakano, M.; Ikeda, T. Directed Bending of a Polymer Film by Light. *Nature* **2003**, *425* (6954), 145.

(14) Hogan, P. M.; Tajbakhsh, A. R.; Terentjev, E. M. Uv Manipulation of Order and Macroscopic Shape in Nematic Elastomers. *Phys. Rev. E: Stat. Phys., Plasmas, Fluids, Relat. Interdiscip. Top.* **2002**, *65* (4), 041720.

(15) Camacho-Lopez, M.; Finkelmann, H.; Palffy-Muhoray, P.; Shelley, M. Fast Liquid-Crystal Elastomer Swims into the Dark. *Nat. Mater.* **2004**, *3* (5), 307−310.

(16) Ikeda, T.; Nakano, M.; Yu, Y.; Tsutsumi, O.; Kanazawa, A. Anisotropic Bending and Unbending Behavior of Azobenzene Liquid-Crystalline Gels by Light Exposure. *Adv. Mater.* **2003**, *15* (3), 201−204.

(17) Sánchez-Ferrer, A.; Merekalov, A.; Finkelmann, H. Opto-Mechanical Effect in Photoactive Nematic Side-Chain Liquid-Crystalline Elastomers. *Macromol. Rapid Commun.* **2011**, *32* (8), 671−678.

(18) Tabiryan, N.; Serak, S.; Dai, X.-M.; Bunning, T. Polymer Film with Optically Controlled Form and Actuation. *Opt. Express* **2005**, *13* (19), 7442.

(19) Harris, K. D.; Cuypers, R.; Scheibe, P.; van Oosten, C. L.; Bastiaansen, C. W. M.; Lub, J.; Broer, D. J. Large Amplitude Light-

Induced Motion in High Elastic Modulus Polymer Actuators. *J. Mater. Chem.* **2005**, *15* (47), 5043−5048.
(20) Küpfer, J.; Finkelmann, H. Nematic Liquid Single Crystal Elastomers. *Makromol. Chem., Rapid Commun.* **1991**, *12* (12), 717−726.
(21) Ichimura, K. Photoalignment of Liquid-Crystal Systems. *Chem. Rev.* **2000**, *100* (5), 1847−1873.
(22) Lee, K. M.; Bunning, T. J.; White, T. J. Autonomous, Hands-Free Shape Memory in Glassy, Liquid Crystalline Polymer Networks. *Adv. Mater.* **2012**, *24* (21), 2839−2843.
(23) de Haan, L. T.; Sánchez-Somolinos, C.; Bastiaansen, C. M. W.; Schenning, A. P. H. J.; Broer, D. J. Engineering of Complex Order and the Macroscopic Deformation of Liquid Crystal Polymer Networks. *Angew. Chem., Int. Ed.* **2012**, *51* (50), 12469−12472.
(24) Ambulo, C. P.; Burroughs, J. J.; Boothby, J. M.; Kim, H.; Shankar, M. R.; Ware, T. H. Four-Dimensional Printing of Liquid Crystal Elastomers. *ACS Appl. Mater. Interfaces* **2017**, *9* (42), 37332−37339.
(25) Kotikian, A.; Truby, R. L.; Boley, J. W.; White, T. J.; Lewis, J. A. 3D Printing of Liquid Crystal Elastomeric Actuators with Spatially Programed Nematic Order. *Adv. Mater.* **2018**, *30* (10), 1−6.
(26) Bisoyi, H. K.; Li, Q. Light-Driven Liquid Crystalline Materials: From Photo-Induced Phase Transitions and Property Modulations to Applications. *Chem. Rev.* **2016**, *116* (24), 15089−15166.
(27) Tanchak, O. M.; Barrett, C. J. Light-Induced Reversible Volume Changes in Thin Films of Azo Polymers: The Photomechanical Effect. *Macromolecules* **2005**, *38* (25), 10566−10570.
(28) Eisenbach, C. D. Isomerization of Aromatic Azo Chromophores in Poly(Ethyl Acrylate) Networks and Photomechanical Effect. *Polymer* **1980**, *21* (10), 1175−1179.
(29) Wen, H.; Zhang, W.; Weng, Y.; Hu, Z. Photomechanical Bending of Linear Azobenzene Polymer. *RSC Adv.* **2014**, *4* (23), 11776−11781.
(30) Lee, W.-E.; Jin, Y.-J.; Park, L.-S.; Kwak, G. Fluorescent Actuator Based on Microporous Conjugated Polymer with Intramolecular Stack Structure. *Adv. Mater.* **2012**, *24* (41), 5604−5609.
(31) Schmidt, B.; Sobotta, C.; Malkmus, S.; Laimgruber, S.; Braun, M.; Zinth, W.; Gilch, P. Femtosecond Fluorescence and Absorption Dynamics of an Azobenzene with a Strong Push−Pull Substitution. *J. Phys. Chem. A* **2004**, *108* (20), 4399−4404.
(32) Asano, T.; Yano, T.; Okada, T. Mechanistic Study of Thermal Z-E Isomerization of Azobenzenes by High-Pressure Kinetics. *J. Am. Chem. Soc.* **1982**, *104* (18), 4900−4904.
(33) Sabourault, N.; Mignani, G.; Wagner, A.; Mioskowski, C. Platinum Oxide (PtO 2): A Potent Hydrosilylation Catalyst. *Org. Lett.* **2002**, *4*, 2117−2119.
(34) Mark, J. E. Some Interesting Things about Polysiloxanes. *Acc. Chem. Res.* **2004**, *37* (12), 946−953.
(35) Blevins, A. A.; Blanchard, G. J. Effect of Positional Substitution on the Optical Response of Symmetrically Disubstituted Azobenzene Derivatives. *J. Phys. Chem. B* **2004**, *108* (16), 4962−4968.
(36) Toro, C.; Thibert, A.; De Boni, L.; Masunov, A. E.; Hernández, F. E. Fluorescence Emission of Disperse Red 1 in Solution at Room Temperature. *J. Phys. Chem. B* **2007**, *112* (3), 929−937.
(37) Taniike, K.; Matsumoto, T.; Sato, T.; Ozaki, Y.; Nakashima, K.; Iriyama, K. Spectroscopic Studies on Phase Transitions in Langmuir−Blodgett Films of an Azobenzene-Containing Long-Chain Fatty Acid: Dependence of Phase Transitions on the Number of Monolayers and Transition Cycles among H-, J-, and J′-Aggregates in Multilayer Films. *J. Phys. Chem.* **1996**, *100* (38), 15508−15516.
(38) Poprawa-Smoluch, M.; Baggerman, J.; Zhang, H.; Maas, H. P. A.; De Cola, L.; Brouwer, A. M. Photoisomerization of Disperse Red 1 Studied with Transient Absorption Spectroscopy and Quantum Chemical Calculations. *J. Phys. Chem. A* **2006**, *110* (43), 11926−11937.
(39) Loucif-Saïbi, R.; Nakatani, K.; Delaire, J. A.; Dumont, M.; Sekkat, Z. Photoisomerization and Second Harmonic Generation in Disperse Red One-Doped and -Functionalized Poly(Methyl Methacrylate) Films. *Chem. Mater.* **1993**, *5* (2), 229−236.
(40) Cheng, L.; Torres, Y.; Min Lee, K.; McClung, A. J.; Baur, J.; White, T. J.; Oates, W. S. Photomechanical Bending Mechanics of Polydomain Azobenzene Liquid Crystal Polymer Network Films. *J. Appl. Phys.* **2012**, *112* (1), 013513.
(41) Kondo, M.; Sugimoto, M.; Yamada, M.; Naka, Y.; Mamiya, J.; Kinoshita, M.; Shishido, A.; Yu, Y.; Ikeda, T. Effect of Concentration of Photoactive Chromophores on Photomechanical Properties of Crosslinked Azobenzene Liquid-Crystalline Polymers. *J. Mater. Chem.* **2010**, *20* (1), 117−122.
(42) Wang, D. H.; Wie, J. J.; Lee, K. M.; White, T. J.; Tan, L. S. Impact of Backbone Rigidity on the Photomechanical Response of Glassy, Azobenzene-Functionalized Polyimides. *Macromolecules* **2014**, *47* (2), 659−667.

DOI: 10.1021/acsami.8b08503
ACS Appl. Mater. Interfaces 2018, 10, 27308−27315